Oxidation of Metals, Vol. 30, Nos. 1/2, 1988

Selective Carbide Oxidation and Internal Nitridation of the Ni–Base Superalloys IN 738 LC and IN 939 in Air

J. Litz,* A. Rahmel,* and M. Schorr*

Received September 8, 1987

Ni-base superalloys contain beside other phases relatively large blocky MC carbides of the type (Ta, Nb, Ti, W)C, which oxidize much faster than the γ/γ' matrix. The large volume increase during oxidation and the oxide formation at the carbide-oxide interface shift the corrosion products outward. High shear stresses between the Cr_2O_3 scale and the carbide oxidation products lead to scale cracking favoring internal corrosion processes in this area. The formation of Al_2O_3 in the subscale is accompanied by a volume increase and tensile stresses in the outer Cr_2O_3 scale. This causes scale cracking and gives nitrogen a chance to enter the metal and form the most stable nitride, TiN beneath the Al_2O_3 subscale.

KEY WORDS: Superalloy; refractory-metal carbide oxidation; internal nitridation; internal oxidation.

INTRODUCTION

The oxidation of Ni-base superalloys has been the subject of various studies.[1-6] The results of earlier publications are summarized by Wasielewski and Rapp.[1] According to the steady-state scale morphology, the precipitation-strengthened Ni-Cr-Al-Ti alloys can be divided into three groups[1]:

Type I: Alloys low in chromium and aluminum contents form a NiO scale with a Cr_2O_3 and Al_2O_3 subscale.

Type II: Alloys high in chromium (>15%) and low in aluminum contents (<3%) form a Cr_2O_3 scale and an Al_2O_3 subscale.

Type III: Alloys high in chromium (>15%) and aluminum contents (>3%) form exclusively an Al_2O_3 scale.

*Dechema-Institut, Postfach 97 01 46, D-6000 Frankfurt am Main 97, Federal Republic of Germany.

0030-770X/88/0800-0095$06.00/0

The scale on IN 939 belongs to type II Cr_2O_3 scale while IN 738 LC ranks between types II and III, depending on the oxidation conditions. This simplification does not consider the oxidation of other elements, such as Ti, Mo, Ta, Nb and of single phases leading locally to a quite different scale morphology. Commercial superalloys have a rather complex structure, depending on the chemical composition of the material. Besides the γ and the γ' phases they contain carbides, nitrides, carbonitrides, and borides. The amount and the size of such precipitates can vary widely, and the size is generally larger in cast than in wrought materials. In particular, cast alloys containing refractory metals, such as Ta, Nb, W, and Mo, form rather large, blocky MC-type carbides having dimensions of a few micrometers. This paper considers two aspects: selective oxidation of the MC carbides and internal nitridation.

EXPERIMENTAL

Specimens with the approximate dimensions $20 \times 10 \times 5$ mm were cut from cast and heat-treated rods of IN 939 and IN 738 LC. The nominal composition is given in Table I. One surface of the specimens was ground and polished to $\frac{1}{4}$-μm diamond. This surface was investigated before and after oxidation in air in a scanning electron microscope (SEM) with an attached energy-dispersive analytical X-ray system (EDA). Metallographic cross sections were also prepared for optical microscopy investigations and electron microprobe analysis (EMPA). The oxidation took place in dry air at 700, 900, and 1100°C. The exposure time varied between 1 and 100 hr. In order to study the selective oxidation of MC carbides, selected surface areas were marked in an optical microscope to investigate them as a function of the exposure time.

RESULTS AND DISCUSSION

Selective Oxidation of MC Carbides

Both materials contain blocky MC carbides. Element mappings revealed that IN 939 contains, in addition to TiC and $M_{23}C_6$, only one (Ta, Nb, Ti, W)C carbide, while IN 738 LC also forms, in addition to these

Table I. Normal Composition of the Alloys Studied (in wt.%)

	C	Cr	Ti	Al	Co	Mo	W	Ni	Nb	Ta
IN 738 LC	0.09	16	3.5	3.3	9	1.8	2.8	bal	1.0	1.8
IN 939	0.15	22	3.8	1.4	20		2.0	bal	1.0	1.3

carbides, small amounts of the types $(Mo, W)_xC_y$, $(Cr, Mo)_xC_y$ and $(Zr, Ti, Nb, Ta)_xC_y$. These last three carbides behave very similar during oxidation to the (Ta, Nb, Ti, W)C carbide and were not considered separately. Small TiC particles act obviously as nuclei for the (Ta, Nb, Ti, W)C carbides, because they can be observed often in these large carbide particles. These carbide particles became selectively oxidized if they are located in or close to the metal surface. The oxidation mechanisms is quite different from that of the metal matrix. The metal matrix forms a protective scale rich in Cr_2O_3. Like the refractory metals, the carbides form a nonprotective scale growing at the oxide-carbide interface. The oxidation causes a large increase in the volume that may be shown by some examples. Examples of ratios of the molar volume V are $V(TiO_2)/V(TiC) = 1.28$ (TiO_2 = rutile); $V(Ta_2O_5)/V(TaC) = 2.23$; $V(Nb_2O_5)/V(NbC) = 2.22$. The different oxidation rates of matrix and carbide, the large volume increase during the oxidation of the carbides and the scale growth at the oxide/carbide interface lead to an outward movement of the carbide oxidation products, as shown schematically in Fig. 1. The development of the scale morphology is given in the series shown in Fig. 2.

This mechanism causes high shear strain at the Cr_2O_3–(Ta, Nb, Ti, W)-oxide interface (Fig. 1). The consequence of this is repeated cracking in such regions, giving aggressive components a chance to enter the metal matrix, thereby causing internal corrosion processes. Another route of

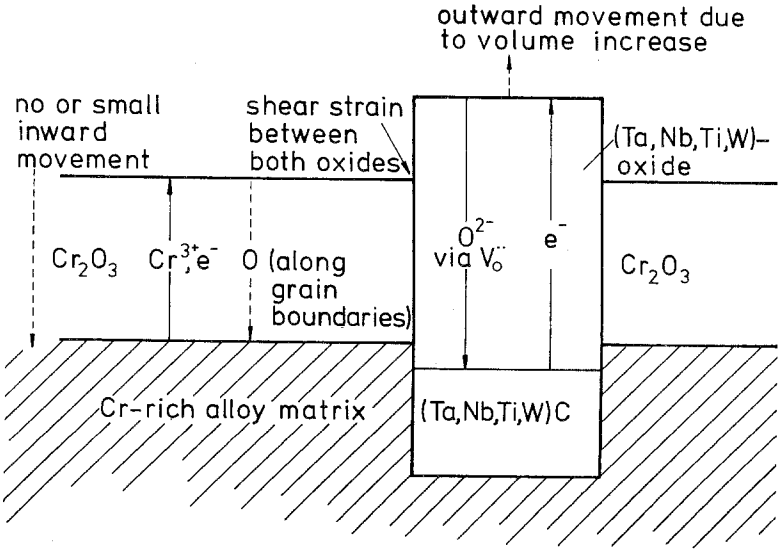

Fig. 1. Schematic scale structure for the matrix and MC.

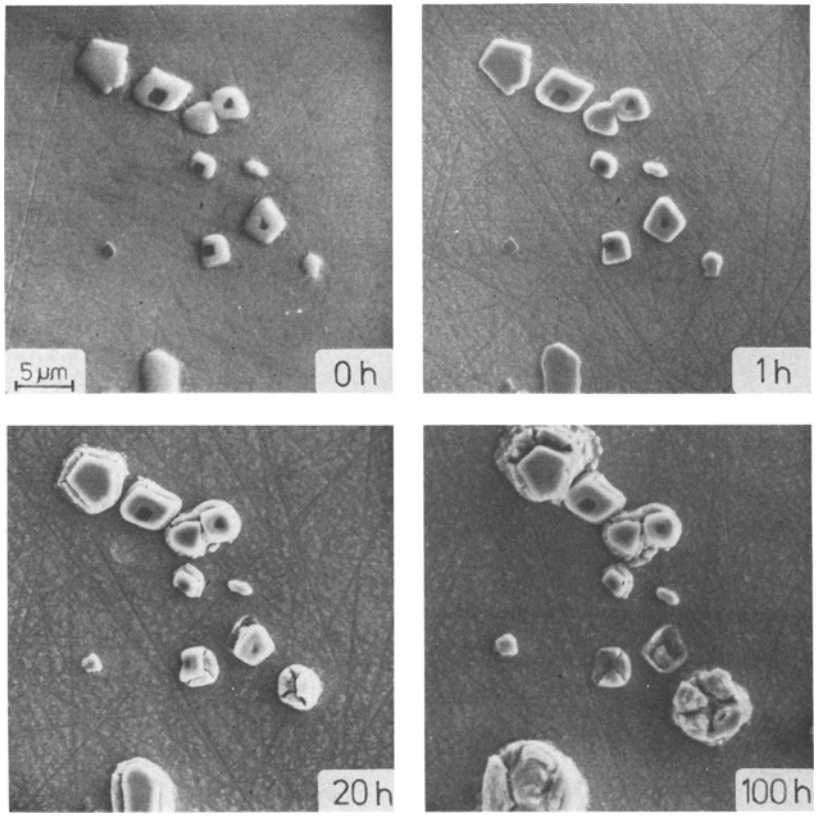

Fig. 2. Development of selective carbide oxidation. IN 939, 700°C, in air.

ingress may be cracks in the (Ta, Nb, Ti, W)-oxide (Fig. 2). These local-scale-damage processes lead to preferential internal corrosion around oxidized carbide particles, as shown schematically in Fig. 3. The element mappings given in Fig. 4 demonstrate the presence of sulfide formation near the oxidized carbide, if the oxidation has been performed with a thin molten Na_2SO_4 deposit on the surface. In some cases, an enhanced internal Al oxidation and a higher Cr_2O_3 scale thickness has been found in such regions. The morphology of the carbide oxidation products as well as the deformation of scale and metal depend obviously on the original carbide particle shape beneath the surface (Fig. 5). A blocky particle with a perpendicular orientation to the metal surface (particle A in Fig. 5) leads to a towerlike outgrowth, as shown in Fig. 6. A large particle beneath the metal surface (particle B in Fig. 5) lifts up the overlaying metal and Cr_2O_3-rich scale (Figs. 7 and 8).

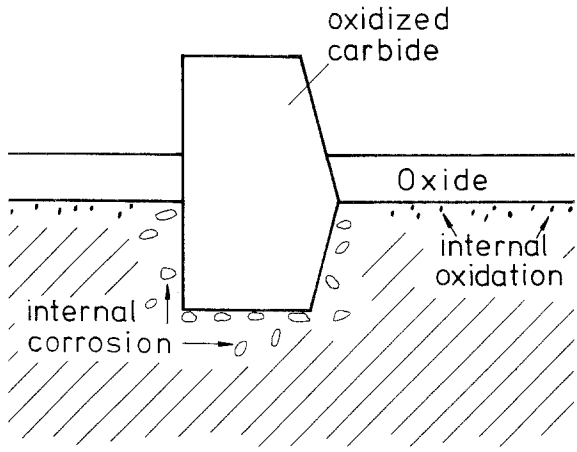

Fig. 3. Schematic diagram of internal corrosion.

At the beginning of the oxidation process, this selective MC oxidation is limited to particles lying on the metal surface. However, when the oxidation front proceeds, the same selective oxidation occurs with those particles which are reached by the oxidation front. Therefore it can be expected that local scale cracking continues during the whole oxidation time.

When the MC particle is completely oxidized, a protective scale, rich in Cr_2O_3, is formed beneath the oxidized particle as follows from the element mappings in Fig. 9, so that the rapid oxidation is stopped. The proceeding metal-matrix oxidation causes the outgrown carbide oxidation products to become incorporated into the scale. These can be identified only by their high local Ta, W, and Ti content. Further changes may occur by solid-state reactions and diffusion.

Internal Nitridation

At temperatures of 900°C and higher both materials suffer internal oxidation by forming Al_2O_3 in the subsurface zone. It is surprising, that this internal oxidation is always accompanied by internal TiN formation beneath the Al_2O_3 subscale if the oxidation has been carried out in air. Typical element mappings are shown in Fig. 10. Nitrogen could not certainly be identified directly by EMPA because the N-Kα line overlaps with the first-order Ti-Lγ line and the second order Co-Lα line. Because of optical microscopy and the absence of O,C and other metals it must be concluded, that these precipitates are TiN.

The internal TiN formation can be prevented if an outer Al_2O_3 scale is developed so that no internal Al_2O_3 subscale can be formed. This is done

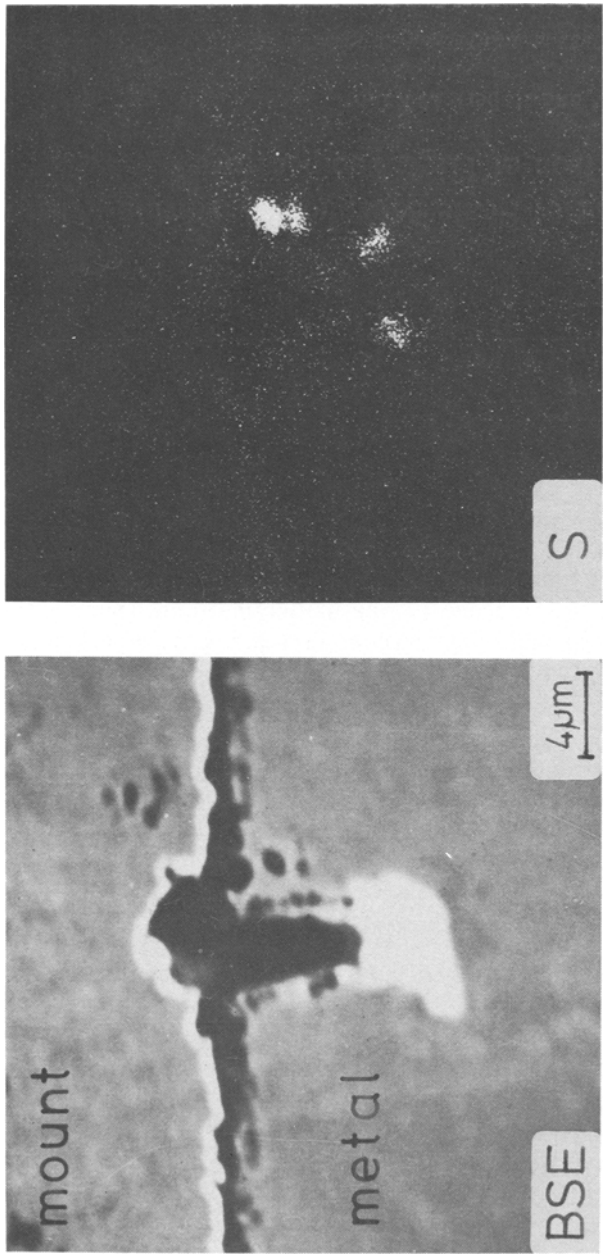

Fig. 4. Element mapping showing internal sulfidation. IN 738 LC, oxidized with Na_2SO_4 deposit, 1 hr, 950°C, in air.

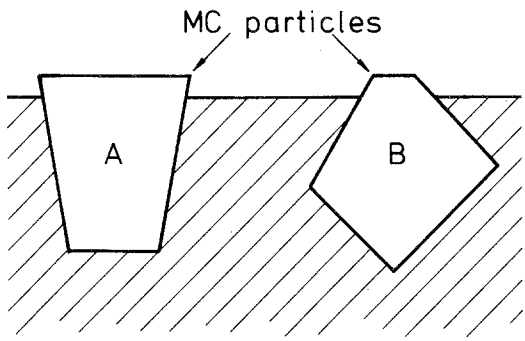

Fig. 5. Examples of carbide shapes beneath the metal surface.

by heating IN 738 LC at 1000°C in argon with traces of impurities, such as CO_2 and H_2O. If the atmosphere is than changed to air without cooling of the specimen, no internal oxidation and nitridation can be found. These observations can be explained as follows: Rapp *et al.*[7] showed that internal oxidation leads to an increase of the volume which causes plastic deformation of the base metal. Rapp *et al.* performed their experiments with Ag–In alloys without an external scale. The formation of Al_2O_3 from Al metal

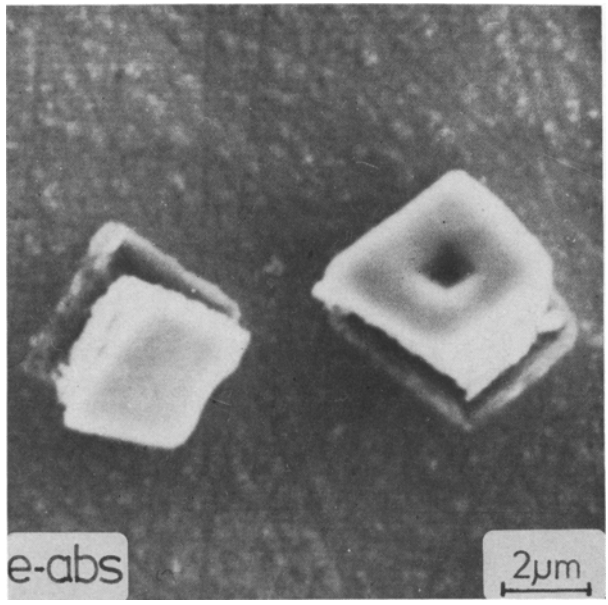

Fig. 6. Towerlike outgrowth of oxidized MC. IN 939, 700°C, 100 hr, in air.

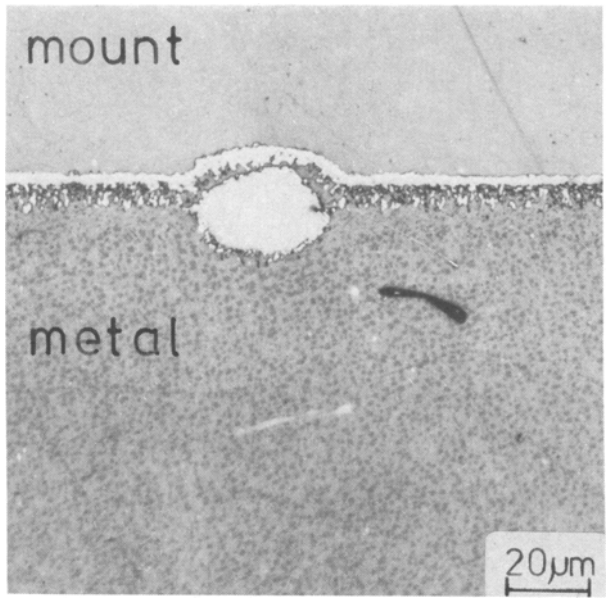

Fig. 7. Metal and scale deformation due to selective carbide oxidation. IN 738 LC, 900°C, 20 hr, in air.

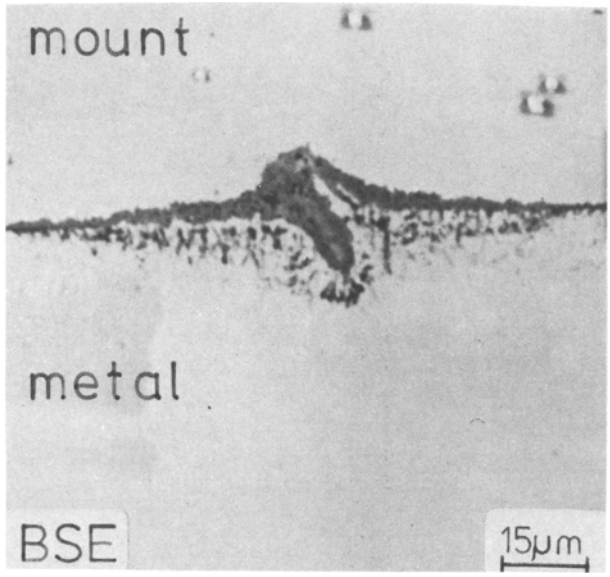

Fig. 8. Cross section showing metal and scale deformation and enhanced internal corrosion due to selective carbide oxidation. SEM, IN 738 LC, 1100°C, 1 hr, in air.

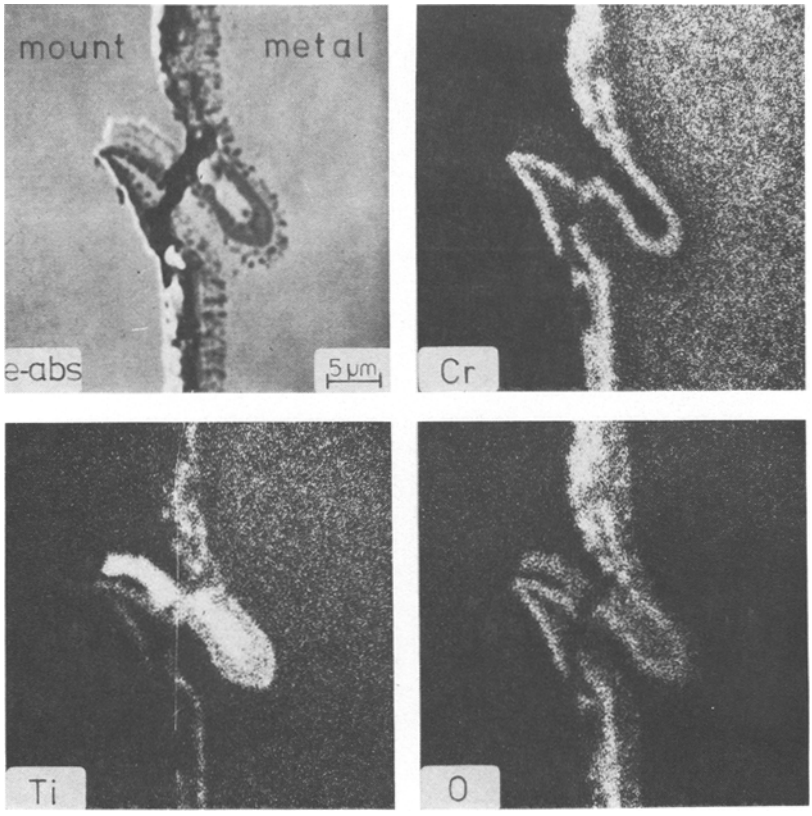

Fig. 9. Element mappings showing protective Cr_2O_3 scale formation beneath oxidized MC. IN 738 LC, 900°C, 20 hr, in air.

causes a volume increase of 28%, the formation of TiN from Ti metal a volume increase of 12%. Compressive stresses are built up in the zone of internal corrosion, while tensile stresses result in the outer scale. The consequence is obviously the formation of microcracks in the outer scale, giving nitrogen the opportunity to enter the metal, forming the most stable nitride TiN.

In a few experiments, a Pt wire of 1-mm thickness was spot-welded to the specimen and connected with a microphone of an acoustic emission (AE) apparatus. The Pt wire acts as a waveguide. The aim of these experiments was to identify scale cracking by their AE-burst signals.[8] These experiments gave no clear evidence of scale cracking. It is conceivable, however, that microcracks grow in small steps releasing only AE signals of small energy and amplitude which cannot be separated from the background noise.

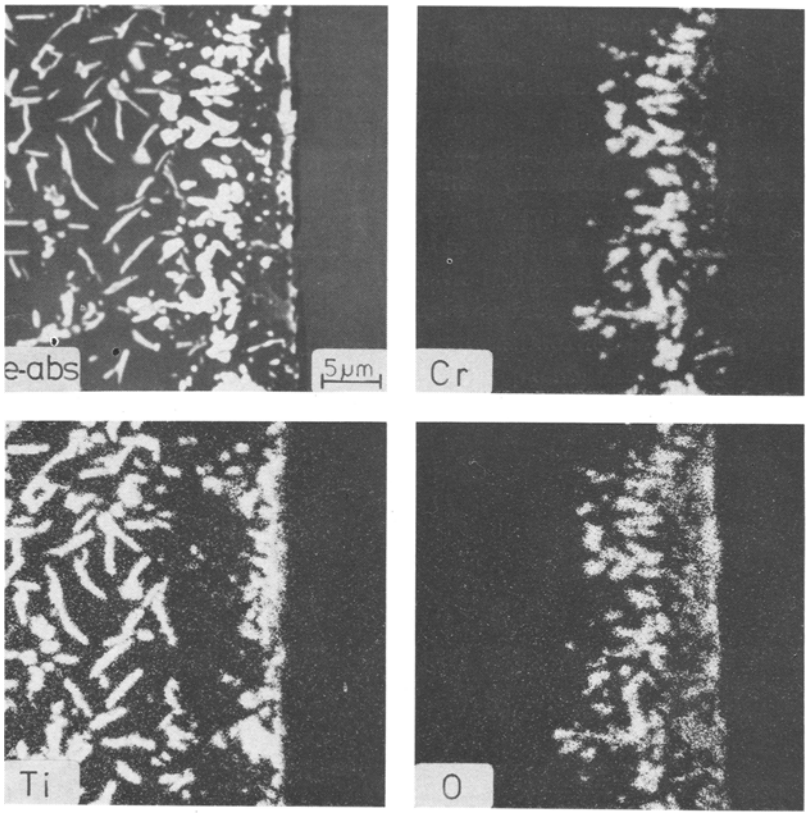

Fig. 10. Element mappings showing internal TiN formation. IN 939, 1100°C, 50 hr.

CONCLUSIONS

Refractory metal carbides such as TiC and (Ta, Nb, Ti, W)C oxidize much faster than the γ/γ'-matrix of the alloy. The large volume increase during the oxidation of these carbides, and the formation of new oxide at the carbide-metal interface lead to an outward movement of the carbide oxidation products. Results are high shear stresses in areas in which the Cr_2O_3 scale and the carbide oxidation products contact, followed by scale cracking and internal corrosion.

The internal oxidation of Al to Al_2O_3 beneath the Cr_2O_3-rich scale causes a volume increase leading to compressive stresses in the internal oxidation zone and to tensile stresses in the scale. These processes lead obviously to scale cracking, giving nitrogen of the air the chance to enter the metal and to form the most stable nitride TiN beneath the Al_2O_3 subscale.

ACKNOWLEDGMENTS

These investigations were sponsored by the Bundesminister für Forschung und Technologie (BMFT). The authors thank the BMFT for the financial support granted.

REFERENCES

1. G. E. Wasielewski and R. A. Rapp, in *The Superalloys*, C. T. Sims and W. C. Hagel, eds. (Wiley, New York, 1972), p. 287.
2. H. J. Christ, L. Berchtold, and H. G. Sockel, *Oxid. Met.* **26**, 45 (1986).
3. C. A. Barrett, G. J. Santoro, and C. E. Lowell, NASA TN D-7484 (1973).
4. C. A. Barrett, J. R. Johnston, and W. A. Sanders, *Oxid. Met.* **12**, 343 (1978).
5. C. A. Barrett, R. V. Miner, and D. R. Hull, *Oxid. Met.* **20**, 255 (1983).
6. F. Abe, H. Araki, H. Yoshida, and M. Okada, *Oxid. Met.* **27**, 21 (1987).
7. S. Guriswamy, S. M. Park, J. P. Hirth, and R. A. Rapp, *Oxid. Met.* **26**, 77 (1986).
8. M. Schütze, *Oxid. Met.* **24**, 265 (1985).